NeuroImage 197 (2019) 512–526

Contents lists available at ScienceDirect

NeuroImage

journal homepage: www.elsevier.com/locate/neuroimage

Decoding of muscle activity from the sensorimotor cortex in freely behaving monkeys

Tatsuya Umeda [a,*], Masashi Koizumi [a], Yuko Katakai [b,c], Ryoichi Saito [b], Kazuhiko Seki [a,**]

[a] Department of Neurophysiology, National Institute of Neuroscience, National Center of Neurology and Psychiatry, Kodaira, Tokyo, 1878502, Japan
[b] Administrative Section of Primate Research Facility, National Institute of Neuroscience, National Center of Neurology and Psychiatry, Kodaira, Tokyo, 1878502, Japan
[c] The Corporation for Production and Research of Laboratory Primates, Tsukuba, Ibaraki, 3050003, Japan

ARTICLE INFO

Keywords:
Marmoset
Brain-Machine Interface
Free movement
Electrocorticogram
Electromyogram

ABSTRACT

Remarkable advances have recently been made in the development of Brain-Machine Interface (BMI) technologies for restoring or enhancing motor function. However, the application of these technologies may be limited to patients in static conditions, as these developments have been largely based on studies of animals (e.g., non-human primates) in constrained movement conditions. The ultimate goal of BMI technology is to enable individuals to move their bodies naturally or control external devices without physical constraints. Here, we demonstrate accurate decoding of muscle activity from electrocorticogram (ECoG) signals in unrestrained, freely behaving monkeys. We recorded ECoG signals from the sensorimotor cortex as well as electromyogram signals from multiple muscles in the upper arm while monkeys performed two types of movements with no physical restraints, as follows: forced forelimb movement (lever-pull task) and natural whole-body movement (free movement within the cage). As in previous reports using restrained monkeys, we confirmed that muscle activity during forced forelimb movement was accurately predicted from simultaneously recorded ECoG data. More importantly, we demonstrated that accurate prediction of muscle activity from ECoG data was possible in monkeys performing natural whole-body movement. We found that high-gamma activity in the primary motor cortex primarily contributed to the prediction of muscle activity during natural whole-body movement as well as forced forelimb movement. In contrast, the contribution of high-gamma activity in the premotor and primary somatosensory cortices was significantly larger during natural whole-body movement. Thus, activity in a larger area of the sensorimotor cortex was needed to predict muscle activity during natural whole-body movement. Furthermore, decoding models obtained from forced forelimb movement could not be generalized to natural whole-body movement, which suggests that decoders should be built individually and according to different behavior types. These results contribute to the future application of BMI systems in unrestrained individuals.

1. Introduction

Significant progress has been made in the development of Brain-Machine Interfaces (BMIs) over the past two decades (Lebedev and Nicolelis, 2017; Moxon and Foffani, 2015). This progress relies heavily on the development of new methodology in the field of neural decoding, in which neuronal activities are translated into signals that can be used to control external devices such as limb prostheses or computers (Lebedev et al., 2008). Currently, movement-related information such as the kinematic parameters of motion, forces, and muscle activity can be accurately decoded from the neuronal activities of behaving animals (Georgopoulos and Carpenter, 2015; Schwartz, 2016). However, previous neural decoding studies using non-human primates have generally been conducted under unnatural conditions, in which most body parts are physically restrained, and only a small subset of movements, such as arm reaching and hand grasping, are studied. Ultimately, the goal of BMI technology is implementation in a non-restrained condition to enable severely disabled individuals to move naturally and freely.

Animal studies have indicated that neuronal coding of limb movement in unconstrained conditions is different from that in constrained conditions. For example, the tuning properties of single neurons in the primary motor cortex (M1) have been reported to vary among movements performed in different working spaces (Aflalo and Graziano, 2006;

* Corresponding author.
** Corresponding author.
E-mail addresses: tumeda@ncnp.go.jp (T. Umeda), seki@ncnp.go.jp (K. Seki).

https://doi.org/10.1016/j.neuroimage.2019.04.045
Received 27 December 2018; Received in revised form 12 April 2019; Accepted 16 April 2019
Available online 20 April 2019
1053-8119/

Caminiti et al., 1990; Griffin et al., 2015) or between movements performed using focal muscles vs. the whole body (Jackson et al., 2007). Thus, it is not clear whether insights obtained from recordings conducted under constrained conditions can be directly applied to the decoding of movement parameters from cortical neuronal activity recorded during more natural movements.

Recent advances in the development of a head-mounted wireless device have demonstrated the possibility of recording neuronal activity in freely-moving animals (Borton et al., 2013; Chestek et al., 2009; Fernandez-Leon et al., 2015; Mavoori et al., 2005; Schwarz et al., 2014). For example, several studies have wirelessly recorded neuronal action potentials from the sensorimotor cortex of rhesus macaques using multi-electrode arrays during arm reaching towards a reward or walking on a treadmill (Capogrosso et al., 2016; Foster et al., 2012, 2014; Rajangam et al., 2016; Schwarz et al., 2014; Yin et al., 2014). In these studies, the modes of motor behavior (e.g., walking or reaching), as well as the specific epoch in each motor behavior (e.g. the flexor or extensor phase during locomotion), were decoded from an ensemble of spiking activities. However, the researchers only examined a small subset of behaviors using specific tasks. Since a hallmark of non-human primates is the rich variety of motor behavior that forms their daily movements (Jaman and Huffman, 2008), neural coding of their natural behaviors can be more informative by recording neuronal signals during free movements in their home cage.

In the present study, we recorded electrocorticograms (ECoGs) from the sensorimotor cortex and electromyograms (EMGs) from forelimb muscles in common marmosets. We used a wireless recording system to record activity as the marmosets moved freely in a cage. The common marmoset is a New World primate species that is considered to be useful as a research subject in the field of neuroscience (Okano et al., 2012; Prins et al., 2014; Walker et al., 2017). The marmoset has several advantages in terms of recording cortical activity during free movement, as follows: 1) as- in humans and rhesus macaques, the cortical sheet in the marmoset is divided into functionally distinct cortical regions (Rosa and Tweedale, 2005); 2) the structure of the marmoset cortex is lissencephalic, which is advantageous for obtaining neuronal signals from the entire cortex using a two-dimensional grid electrode (Komatsu et al., 2017; Newman et al., 2009; Tia et al., 2017); 3) marmosets are much smaller than rhesus macaques, and are thus easier to handle (Prins et al., 2017); 4) the marmoset shows a wide variety of movements in three-dimensional space, such as walking, jumping, and grasping a pole located in the cage (Wang et al., 2014). Thus, we consider the common marmoset to be optimal for our research.

Here, we demonstrated that accurate prediction of EMG from ECoG is possible during natural whole-body movement of marmosets freely moving in a large space, as well as during forced forelimb movement. While high-gamma activity in the M1 contributed most strongly to the prediction of muscle activity in both movement types, a larger area of the sensorimotor cortex contributed to decoding for natural whole-body movement than for forced forelimb movement. These results provide insights that are relevant to future applications of BMI systems in unrestrained individuals.

2. Materials and methods

We used three adult female monkeys (*Callithrix jacchus*, weight 380–510 g) in the present study. The experiments were approved by the experimental animal committee of the National Institute of Neuroscience. All animals were cared for and treated humanely in accordance with the institutional guideline for experiments using animals and the NIH guidelines. Before the experiments, the animals were housed with their family with a 12-h light/dark cycle.

2.1. Lever-pull task

Within the experimental cage, all the monkeys were trained to perform a lever-pull task with the right (Monkeys J and H) or left (Monkey S) hand. The task involved a lever that was connected to a spring that exerted a force (0.049 N/mm in Monkey J, 0.024 N/mm in Monkeys H and S) in the direction opposite to the movement of the lever. The monkeys were trained to grasp the lever, pull it closer to get a reward, and then release it. To receive a reward, they had to pull the lever towards them by 1 cm (Monkey J) or 2 cm (Monkeys H and S). The monkeys were not physically constrained during the task. We recorded the time at which they started to pull the lever using a sensor. Monkey J completed five recording sessions (duration of sessions: 8.3–12.5 min; number of trials within each session: 140–164 trials), Monkey H completed seven sessions (9.2–10.8 min; 155–302 trials), and Monkey S completed six sessions (8.3–11.7 min; 101–200 trials).

2.2. Free movement

We recorded ECoG and EMG signals from Monkeys H and S as they freely moved in the experimental cage (width 30 cm, depth 50 cm, and height 60 cm). They typically walked, vertically climbed, jumped, and groomed themselves. They also reached to grasp a small piece of marshmallow that was offered to them. While recording ECoG and EMG signals during the free movement in the cage, we took a video of the monkeys' behaviors from the front using a video camera (GZ-E765, Japan Victor Company, Yokohama, Japan). From a video image, we crudely marked the time of onset and termination of each behavior with an aid of ELAN5.3 (Max Planck Institute for Psycholinguistics, Nijmegen, Netherlands) (Walker et al., 2018). Then, we precisely determined the time of onset of each behavior by assigning it with the onset of the bursting activity of deltoid (Del) (see section 2.4. Recordings and preprocessing). The monkeys exhibited variable numbers and durations of the different behaviors (Supplementary Tables 1 and 2). ECoG and EMG signals were recorded from Monkey J while the monkey freely moved in a ladder apparatus (width 30 cm, depth 30 cm, and height 120 cm). The monkey climbed a vertical ladder that was 120 cm tall to reach the top of the apparatus, where she entered a box to receive a reward. After the monkey had entered the box, an experimenter moved the monkey to the bottom of the ladder. The monkey jumped, climbed, and walked in the apparatus, and grasped a reward (a small piece of marshmallow) using her hand. Monkey J completed four recording sessions (duration of sessions: 12.5–26.7 min), Monkey H completed six sessions (28.3–30.8 min), and Monkey S completed seven sessions (29.2–33.3 min).

2.3. Surgery

After the completion of behavioral training, we separately performed two surgeries. In the first surgery, a grid electrode array was implanted on the cortical surface. In the second surgery, wire electrodes were implanted into multiple forelimb muscles. The second surgery was performed after a sufficient recovery period (at least two weeks). In both surgeries, we used a mixture of xylazine (0.4 mg/kg) and ketamine (20 mg/kg) to induce anesthesia in the monkeys, and then used isoflurane (exhaled level: 1–2%) to maintain anesthesia. Electrocardiograms, percutaneous oxygen saturation levels, and expiratory CO_2 levels were continuously monitored. The depth of anesthesia was monitored according to expiratory CO_2 levels and heart rate. We postoperatively administered dexamethasone, ketoprofen, and ampicillin.

To implant a grid electrode array on the cortical surface, we made a craniotomy to expose the premotor cortex, M1, and primary somatosensory cortex (S1) on the left (Monkeys J and H) or right (Monkey S) hemisphere. We implanted a 32-channel grid electrode array in which the diameter of each electrode was 0.2 mm, and the inter-electrode distance was 1 mm (Neuronexus, Ann Arbor, MI) beneath the dura mater (Fig. 1A). The two reference electrodes were placed between the dura and skull. One reference electrode was placed posterior to the electrode array, and the other was placed anterior or lateral to the electrode array.

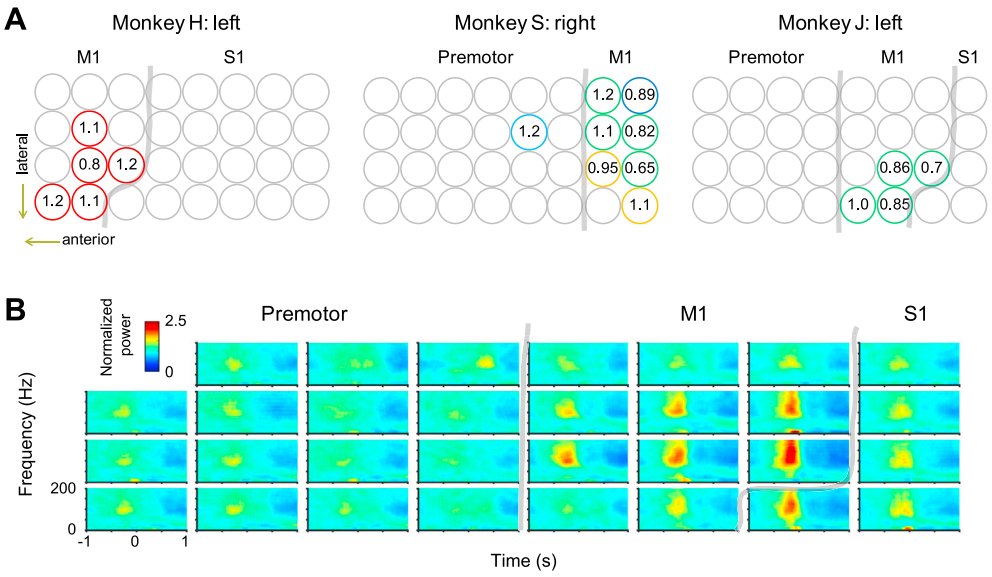

Fig. 1. Electrocorticogram (ECoG) electrode locations over the sensorimotor cortex of the common marmoset. (**A**) Schematic diagrams of ECoG electrode locations in the three monkeys. All monkeys had a 32-channel subdural grid electrode array over the sensorimotor cortex. The grid electrode array was placed on the left hemisphere in Monkeys H and J, and the right hemisphere in Monkey S. Circles represent the locations of electrodes, with threshold currents (in mA) and specific evoked movements (Shoulder: green; Elbow: orange; Wrist: red; Hindlimb: blue; Neck: cyan). (**B**) Spectrograms of the corresponding recording sites in the lever-pull task for Monkey J. All signals were aligned to the time of pulling the lever. We detected a movement-related component of cortical activity in the sensorimotor cortex and found that the magnitude of this component was higher in the M1 than in other cortical regions.

After implanting the array, we fixed a connector onto the skull via dental acrylic.

Two to three weeks after the implantation of the grid electrode array, we secured pairs of Teflon insulated wire electrodes of 0.279 mm diameter (AS631; Cooner Wire, Chatsworth, CA) in the forelimb muscles of the right (Monkeys J and H) or left (Monkey S) side using silk sutures (Loeb and Gans, 1986). After we physically removed the coating shield of Teflon insulation for about 1 mm by a sharp knife, we implanted wire electrodes in the Del, triceps brachii (TB), biceps brachii, extensor carpi radialis (ECR), flexor digitorum superficialis (FDS), and flexor carpi radialis (FCR). We confirmed the location of each EMG implant during surgery by evoking joint and muscle movement via low-intensity electrical stimulation applied through the wire electrodes.

2.4. Recordings and preprocessing

ECoG and EMG signals were amplified using a wireless head-mounted transmitter (W64 system; Triangle Biosystems International, Durham, NC) with a gain of × 800 and sampling rate of 2000 Hz for each electrode. ECoG signals in the present wireless recording were contaminated with the low-frequency noise related to the animal's movement presumably due to no connection of the animals' body to the ground. For this reason, we applied a second-order Butterworth bandpass filter (10–240 Hz). Even after the filtering, large noise occasionally appeared in some or most of the electrodes at the same time. This type of noise was most likely generated by the transient contact failure between connectors by the mechanical contact of the transmitter to the inner wall of a marmoset cage. To eliminate these transient large artifacts, we first detected them by setting a large threshold (ten times the standard deviation of the total recorded signal in a single session), and if signal amplitude exceeded this threshold we interpolated the median value of the total recorded signal in the session to the epoch of 40 ms starting before 15 ms of the occurrence of the noise. Then, we computed short-time fast Fourier transforms on moving 200-ms windows of the preprocessed signal. We used a step size of 200 Hz to match the sampling rate of the preprocessed EMG signals. Fig. 1B shows an example of a time-frequency spectrogram of the cortical activities in the sensorimotor regions in the lever-pull task in Monkey J. We computed the power of each frequency normalized to the averaged power of that frequency in each session and calculated the averaged power in the beta (15–35 Hz), gamma (35–60 Hz), and high-gamma (60–180 Hz) bands. In Monkey J, ECoG data from one channel were not transmitted due to the configuration of a connector on the transmitter. Thus, we recorded signals from 31 channels in this animal.

We carried out the temporal filtering of the EMG signals using a second-order Butterworth high pass filter (200 Hz) to remove the electrocardiogram signal. The EMG signals were rectified and computed in 5-ms bins. When the EMG signals were preprocessed with a small smoothing window, the present decoding method using ECoG signals failed to reconstruct rapid EMG fluctuations (Supplementary Fig. 1A). Since the prediction accuracy increased and then reached a plateau at around 41 bins (200 ms, Supplementary Fig. 1B and C) and a similar filtering parameter has often been used to extract the EMG envelope in previous literature (Flint et al., 2012a; Shin et al., 2012), we calculated the smoothed curves for the signals using a mobile window process with a length of 41 bins. We used EMG signals in which there was no detectable noise. Some EMG signals were obtained from a single wire electrode and amplified relative to ground (single-ended recording), and other signals were obtained from the differentiation between two electrodes inserted into the same muscle (differential recording). We quantified the extent of electrical cross-talk between EMG signals recorded from different muscles using the method developed by Kilner et al. (2002). We calculated cross-correlation functions between third-order differentiated raw EMG signals. If the maximum value exceeded 0.25 in each muscle pair, one muscle was eliminated from the data pool. After the selection, we used signals from the Del, TB, ECR, and FDS in Monkey J, Del, and FDS in Monkey H, and Del, FCR, and FDS in Monkey S for further analysis.

To assess the variability of the EMG profile, we further carried out the temporal filtering of the preprocessed EMG signals with a second-order Butterworth low pass filter (2 Hz). If the low-pass signal was above the threshold (0.05 mV) in 50 consecutive bins, the first bin in which the activity was over the threshold was set as the onset of the activity and the first subsequent bin in which the activity was below the threshold was set as the end-point of the activity. We measured the duration of the activity and the maximum value of the preprocessed EMG signals during the activity period. We then calculated the coefficient of variation (CV) for both the duration of the activity and the maximum amplitude as indices of variability in the shape of the EMG profile. Since the ECR amplitude in Monkey J was below the threshold for most of the recording sessions, data regarding the activity of this muscle were not used in our assessment.

2.5. Extraction of the covarying activity between recorded EMGs

To extract the covarying activity across the muscles, we applied nonnegative matrix factorization (NNMF) to the activity of all the muscles that were normalized with the mean of each activity (Tresch et al., 2006). To extract muscle synergies using the NNMF algorithm, the number of output components has been determined based on the variance accounted for (VAF) value between the original EMGs and the reconstructed EMGs from output components, as follows:

$$\mathrm{VAF}\ (\%) = \left(1 - \frac{\sum (y(t) - c(t))^2}{\sum \left(y(t) - \overline{y(t)}\right)^2}\right) \times 100 \quad (1)$$

where $y(t)$ is a vector of the actual muscle activities from the recorded muscles at time index t. $\overline{y(t)}$ is the mean of $y(t)$. $c(t)$ is the muscle activity calculated from output components at time index t. We also determined the number of components based on the conventional VAF value for extracting muscle synergies (more than 80%) (Cheung et al., 2012; Takei et al., 2017). We set the number of NNMF components to one for Monkey H, two for Monkey S and three for Monkey J in forced forelimb movement and one for Monkey H, and two for Monkeys S and J in natural whole-body movement (Supplementary Fig. 2).

2.6. Identification of cortical regions

After anesthetizing the monkeys using ketamine (20 mg/kg), we performed cortical motor mapping by monopolar stimulation through the grid electrode array at 2 Hz using an electrically isolated, constant current stimulator (SEN-3401, Nihon Kohden, Tokyo, Japan). Individual stimulus trains consisted of 12 symmetrical biphasic pulses at 333 Hz, with a 0.1-ms negative pulse followed by a 0.1-ms positive pulse. The stimulating current was increased gradually until joint and muscle movements could be detected. The minimum current required to elicit movements was recorded as the motor threshold. If no movements or twitches were evoked at 1.2 mA, the site was defined as "nonresponsive". We identified the cortical regions based on both the distribution of the motor threshold and the marmoset brain atlas (Burish et al., 2008) (Fig. 1A).

2.7. Decoding using sparse linear regression (SLiR)

We used multidimensional linear regression to model EMG signals as a weighted linear combination of ECoG signals, as follows:

$$y(t) = \sum_{k,j} w_{k,l} \times x_k(t + l\delta) + b \quad (2)$$

where $y(t)$ is a vector of the EMG signal from a single muscle at time index t. $x_k(t + l\delta)$ is an input vector of ECoG signal k (32 or 31 channels x three frequency bands) at time index t and time lag $l\delta$ ($\delta = 5$ ms). $w_{k,l}$ is a vector of weights on ECoG signal k at time lag $l\delta$ (referred to as model), and b is a vector of the bias term associated with y. We applied a Bayesian SLiR algorithm that introduced sparse conditions for the channel dimension only, and not for the temporal dimension of the model. The SLiR automatically and efficiently extracted appropriate feature sets and discarded less essential signals for many explanatory variables to achieve a better generalization performance compared with the regularized linear model (Ganesh et al., 2008). The methodology estimated the weight and the automatic relevance determination parameters that represented the degree to which the weight contributed to the reconstruction. Relevant features were selected automatically and unnecessary features were pruned according to automatic relevance determination parameters. Since the muscle activity is evoked by neuronal activity, we set the time lag $l\delta$ (Equation (2)) to negative values. We used ECoG signals from −500 ms to time 0 to decode muscle activity at time 0 (see Supplementary Results for Setting of the decoding parameters).

We divided continuously-recorded data into 50-s epochs. Of these data epochs, eight epochs were used for generating a model to predict muscle activity from ECoG data (training data set; see Supplementary Results for Setting of the decoding parameters). Performance of these models was assessed by calculating the correlation coefficient between actual and predicted muscle activities in two epochs (test data set) that were selected randomly from the residual data epochs. We also calculated the fraction of variance accounted for (FVAF) between actual and predicted muscle activities in the test data set, as follows:

$$\mathrm{FVAF} = 1 - \frac{\sum (y(t) - f(t))^2}{\sum \left(y(t) - \overline{y(t)}\right)} \quad (3)$$

where $y(t)$ is a vector of the actual muscle activity from a single muscle at time index t. $\overline{y(t)}$ is the mean of $y(t)$. $f(t)$ is the predicted muscle activity at time index t. We performed a 5-fold cross-validation.

To obtain a baseline of the decoding results, we performed identical procedures on a surrogate training data set that was generated by random shuffling of temporal profiles of inputs independently across different sessions to generate a model.

To obtain the generalization performance, we applied models that were built from data in a different session for the same movement, or data for another type of movement, to the test data set. We calculated the correlation coefficient and FVAF between actual and predicted muscle activities in the test data set for each model and obtained the average of correlation coefficient and FVAF. We considered that the models had a high generalization capability if both the correlation coefficient and FVAF were statistically higher than those obtained from surrogate shuffled control data.

SLiR can be used to discard less important signals for many explanatory variables; we assigned a weight value of zero to the less important inputs. We calculated the proportion of selected channels for each frequency band. Additionally, we calculated the proportion of selected channels for each frequency band in each cortical region. Finally, we calculated the average of the weight values for each channel in the model for the prediction of each muscle to assess the contribution of each channel to decoding.

2.8. Statistical analysis

The data were analyzed using paired Student's t-tests. An alpha level of significance was set at 0.05 for all statistical tests. Data are expressed as the mean ± standard error (mean ± S.E.) or the mean ± standard deviation (mean ± S.D.). We used Matlab R2015b (Mathworks, Natick, MA) for statistical analysis. No statistical methods were used to predetermine sample sizes. However, these sample sizes have been estimated by previous methodologically comparable experiments in the laboratory.

2.9. Data availability

The data that support the findings of this study are available from the corresponding author, T.U., upon reasonable request.

3. Results

3.1. Cortical and muscle activities were simultaneously recorded from marmosets

Fig. 2A shows simultaneously recorded forelimb muscle activity and cortical oscillatory activity that occurred while a monkey pulled the lever. EMG data from proximal and distal forelimb muscles showed the following profile: activity of Del had a single peak around the time at which the monkey pulled the lever, activity of TB showed the first peak around movement onset and a second around the time at which the lever

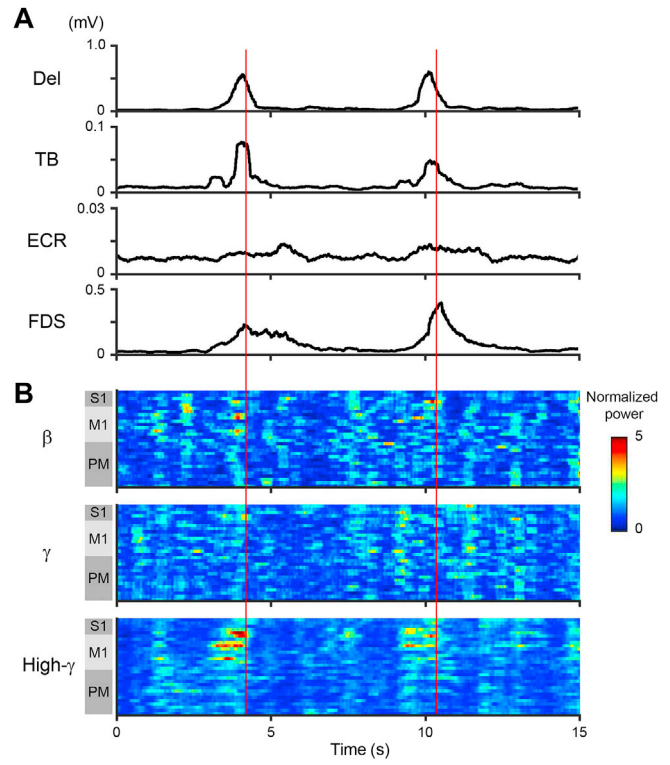

Fig. 2. Example of simultaneous recording of electromyogram (EMG) and ECoG signals during forced forelimb movement. (**A**) EMG signals from the shoulder (Del), arm (TB), wrist (ECR) and hand (FDS) muscles for two trials of the lever-pull task by Monkey J. (**B**) Signal power in specific frequency bands of the ECoG signals from 31 electrodes. Red vertical lines represent the time of pulling the lever. PM: premotor cortex.

was pulled, there was almost no activity of ECR, and activity of FDS showed a sustained activity compared with that for the proximal muscles. As shown in Fig. 2B, ECoG signals recorded from some of the electrodes exhibited movement-related modulation. For example, both beta (15–35 Hz) and high-gamma (60–180 Hz) activities in the M1 showed modulation during movement, while gamma (35–60 Hz) activity in the sensorimotor cortex did not show significant movement-related activity in Monkey J.

Fig. 3 shows simultaneous recordings of both EMG and ECoG signals while a monkey moved freely in the cage. The monkey exhibited various behaviors such as walking on the floor, jumping between sidebars and the floor, and climbing down from bars to the floor in the cage (Fig. 3A). The activity of Del tended to be large during jumping compared to during walking. As expected, natural whole-body movement in the cage (Fig. 3A) had a more variable EMG profile than did forced forelimb movement (Fig. 2, Supplementary Fig. 3). High-gamma activity in the M1 and S1 showed movement-related modulations, while beta and gamma activities in the sensorimotor cortex did not (Fig. 3B). Movement-related modulations of high-gamma activity were seen across a larger area than the modulation during forced forelimb movement (Fig. 2).

3.2. *ECoG signals encode muscle activity during forced forelimb movement*

We examined whether the sensorimotor cortex of marmosets encodes muscle activity during forced forelimb movement, as reported previously in restrained animals (Cherian et al., 2011; Flint et al., 2012a; Morrow and Miller, 2003; Pohlmeyer et al., 2007; Shin et al., 2012). For this purpose, we applied the SLiR algorithm to the decoding of muscle activity from the power in the beta, gamma, and high-gamma bands of the ECoG signals. Fig. 4A shows the results of a prediction of proximal and distal forelimb muscle activities in a test data set. The predicted muscle activity reconstructed the single peak of Del activity at around the time of pulling the lever and the sustained activity of FDS. The accuracy of the prediction of all muscles from ECoG data, as measured by the correlation coefficient and FVAF, was much better than that obtained from surrogate shuffled control data (Fig. 4B and C, $p < 0.05$). Thus, the sensorimotor cortex of unrestrained marmosets appears to encode the activity of forelimb muscles during forced forelimb movement.

3.3. *ECoG signals encode muscle activity during natural whole-body movement*

Next, we examined whether the sensorimotor cortex of marmosets encodes muscle activity during natural whole-body movement. Fig. 5A shows the results of a prediction of activity in two forelimb muscles from

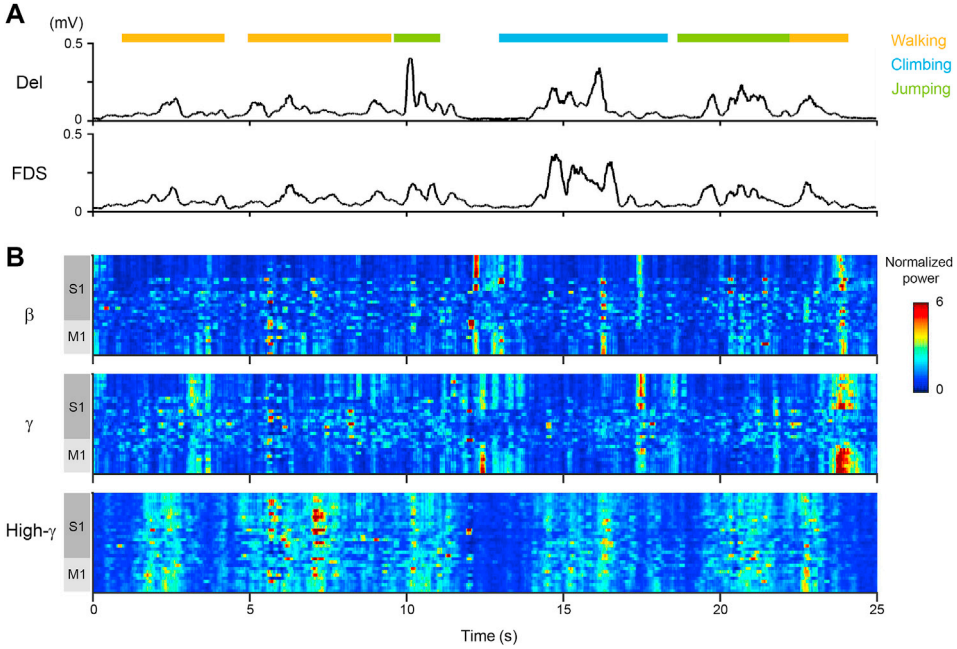

Fig. 3. Example of simultaneous recording of EMG and ECoG signals during natural whole-body movement. (**A**) EMG signals from the shoulder (Del) and hand (FDS) muscles of Monkey H. (**B**) Signal power in specific frequency bands of the ECoG signals from 32 electrodes. Orange bars represent the period during which the monkey walked on the floor, the cyan bar indicates when the monkey vertically climbed the wall in the cage, and green bars show when the monkey jumped between the bars and the floor.

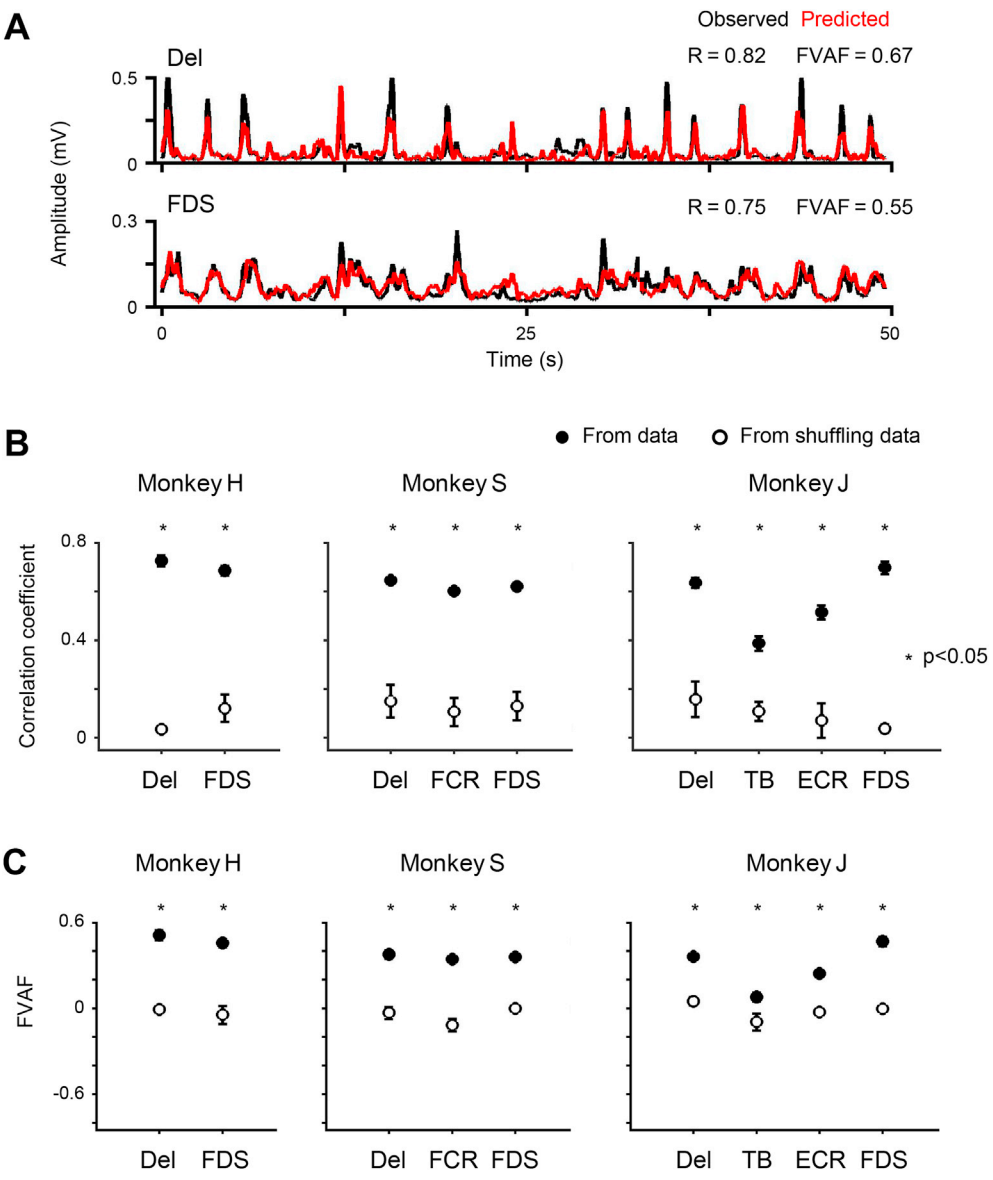

Fig. 4. Prediction of muscle activity from cortical activity during forced forelimb movement. (**A**) Reconstruction of the shoulder (Del) and hand (FDS) muscle activities using ECoG signals (Monkey H, the lever-pull task). Black and red traces show the observed and predicted EMG profiles. The correlation coefficient (R) and the fraction of variance accounted for (FVAF) between the observed and predicted EMG profiles are shown in the upper right corner of each graph. (**B**, **C**) Mean accuracy of the prediction of each muscle activity. The filled circles depict the correlation coefficient (B) and the FVAF (C) between the actual and predicted profiles from the data. The open circles depict the correlation coefficient (B) and FVAF (C) between the actual EMG profile and the profile predicted from random shuffling of ECoG signals. Error bars represent the S.E. $^{*}p < 0.05$ (adjustments for multiple testing using the Holm method (n = 2; correlation coefficient and FVAF)).

an ECoG test data set. The predicted muscle activity reconstructed the phasic pattern of muscle activity during jumping and sustained activity during walking. The accuracy of the prediction of all muscles from ECoG data was much better than that obtained from surrogate shuffled control data (Fig. 5B and C, Monkeys H and S, $p < 0.05$). In addition, we trained one monkey to climb a vertical ladder, which is more object-oriented, innate behavior of marmoset. The model that predicted muscle activity from the ECoG data recorded during the task also accurately reconstructed the overall temporal EMG pattern more effectively than a model constructed from surrogate shuffled control data (Fig. 5B and C, Monkey J, $p < 0.05$). Overall, our method accurately decoded muscle activity from ECoG data recorded during natural whole-body movement.

3.4. *ECoG signals encode muscle-specific activity as well as the covarying activity between multiple muscles*

Some of the recorded muscles exhibited a more or less comparable temporal pattern in their activity for both forced forelimb and natural whole-body movements (Figs. 2 and 3). We tested whether ECoG signals encode the covarying components between multiple muscles. For this, we extracted the covarying component by applying NNMF to all the muscles and tested if the extracted components could be decoded by ECoG signals. Fig. 6A and D shows the results of a prediction of the covarying component from an ECoG test data set during forced forelimb movement and natural whole-body movement, respectively. For both movements, the accuracy of the prediction of most of the covarying components from ECoG data was much better than that obtained from surrogate shuffled control data (Fig. 6B, C, E, and F, $p < 0.05$). This suggests that the covarying components across the muscles are indeed encoded by the ECoG signals in both movements.

Next, we examined if the ECoG signals could also encode the muscle-specific component intrinsic to each muscle, not only the covarying components among multiple muscles. For this purpose, individual muscle activity was reconstructed using (1) the models obtained from the covarying components and (2) the models obtained from the individual muscle activity, and compared the accuracy of prediction between them. The rationale of which is that if the ECoG signals do not encode the muscle-specific components, the decoding performance of the latter model (2) is equivalent to the former model (1). Results for the forced forelimb and natural whole-body movements are shown in Fig. 7. We found that the accuracy of prediction was significantly lower ($p < 0.05$) when the covarying components were used to build the model in 67% (6

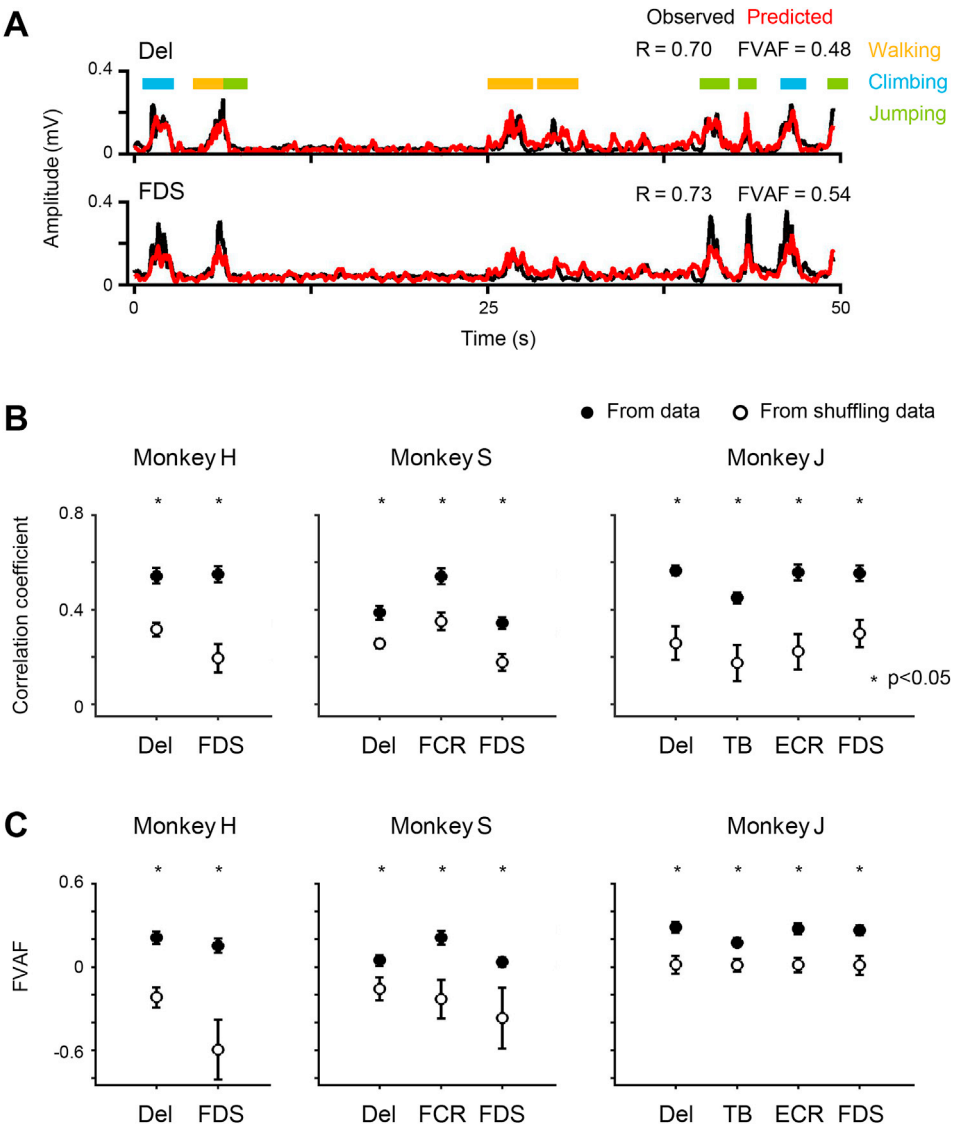

Fig. 5. Prediction of muscle activity from cortical activity during natural whole-body movement. (**A**) Reconstruction of the shoulder (Del) and hand (FDS) muscle activities using ECoG signals (Monkey H, free movement in the cage). Black and red traces show the observed and predicted EMG profiles. The orange bar represents the period during which the monkey walked on the floor, the cyan bar indicates when the monkey climbed up the sides of the cage, and green bars show when the monkey jumped between the bars and the floor. The correlation coefficient (R) and FVAF between the observed and predicted EMG profiles are shown in the upper right corner of each graph. (**B**, **C**) The diagrams use a similar format for Fig. 4B and C.

out of 9) of all the recorded muscles in the forced forelimb movement (Fig. 7A–C) and 11% (1 out of 9) of the recorded muscles in the natural whole-body movement (Fig. 7D–F). Regarding the context of movement performed by the monkeys, this difference between the two conditions is expected and reasonable. During the natural whole-body movement, for example, the monkeys spent a majority of the recording period performing several types of stereotyped behavior (e.g. locomotion, jumping, and sitting) which mainly involves synergistic control of multiple muscles. On the other hand, to perform the forced forelimb movement, the monkeys need to activate multiple muscles in a rather different way to match the end-point force with the task requirement. Consequently, ECoG signals more preferentially encoded muscle-specific information in the forced forelimb movement. Overall, the results suggest that ECoG signals could encode both the covarying component among muscles and the muscle-specific component for individual muscles.

3.5. *High-gamma activity in the primary motor cortex significantly contributes to decoding accuracy*

Next, we compared the decoding performance between three different frequency bands of ECoG signals (beta, gamma, and high-gamma). We explored the proportion of channels that were selected by the SLiR for each frequency band. For both forced forelimb and natural whole-body movements, the activity within the high-gamma frequency band was more frequently selected than that for other frequency bands (Fig. 8, Supplementary Table 3). This suggests that the high-gamma activity could be more informative than other frequency bands. To validate this result, we examined the most informative frequency band by building a model from the signal power of individual frequency bands. Consequently, we found the model using high-gamma activity provided a more accurate prediction than those from other frequency bands (Supplementary Fig. 4, $p < 0.05$) for both forced forelimb and natural whole-body movements. Thus, high-gamma activity in the sensorimotor cortex encodes muscle activity during natural whole-body movement as well as forced forelimb movement in unrestrained marmosets.

Next, we identified the ECoG electrode that predominantly contributed to the decoding output by analyzing the weight value of the high-gamma activity in each channel for both forced forelimb (Fig. 9A) and natural whole-body movements (Fig. 9C). Channels with positive values were predominantly located in the M1. In decoding activity of most of the muscles (67% during forced forelimb movement and 89% during natural whole-body movement), the channel with the highest positive value was in the M1 for both forced forelimb and natural whole-body movements (Fig. 9B and D). However, the locational bias of weight values was not

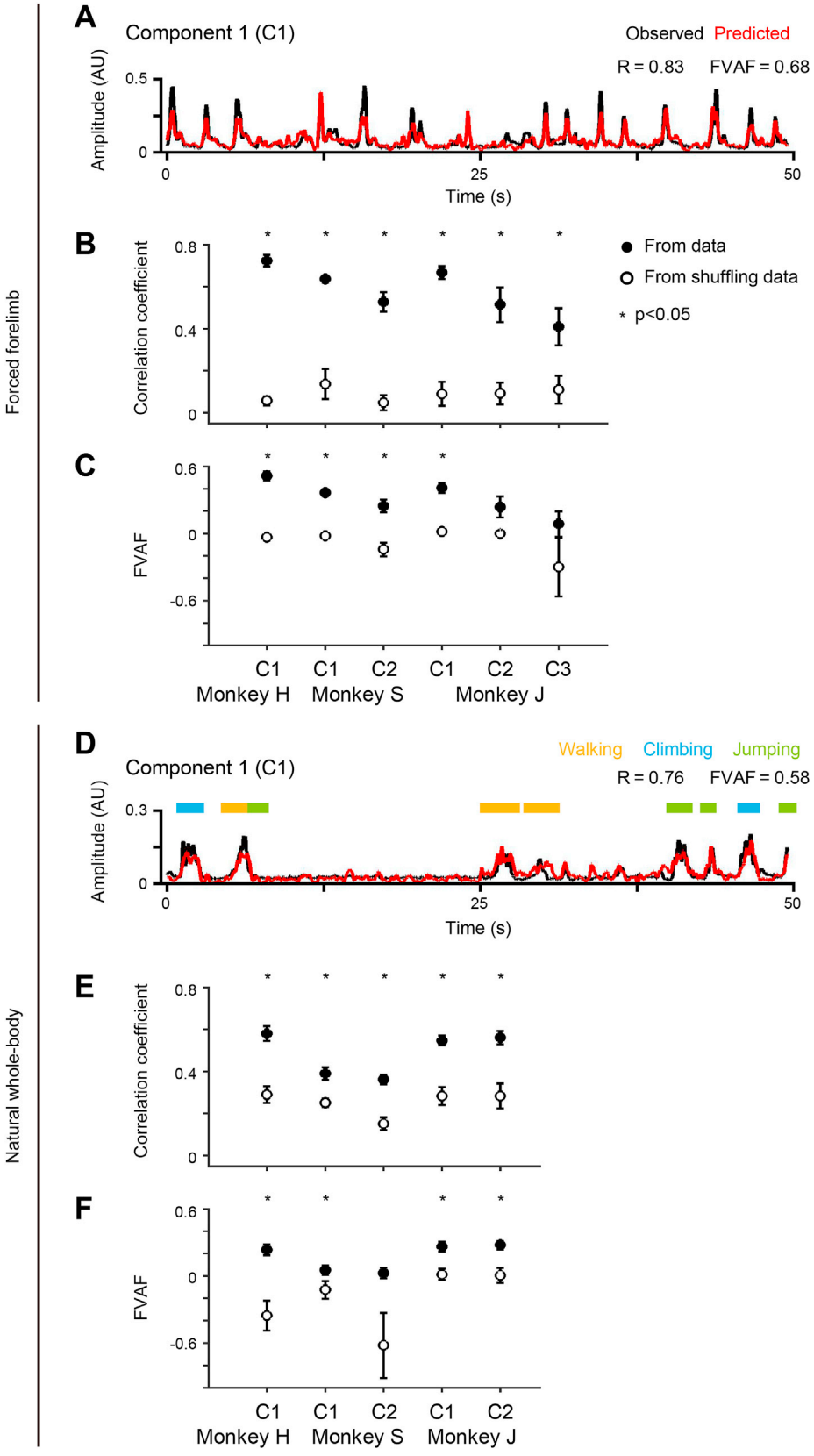

Fig. 6. Prediction of the covarying component shared by multiple muscles from the cortical activity. (A) Reconstruction of the covarying component of EMGs using ECoG signals during forced forelimb movement (Monkey H, the lever-pull task). Black and red traces show the observed and predicted covarying components. The correlation coefficient (R) and FVAF between the observed and predicted covarying components are shown in the upper right corner of each graph. (**B**, **C**) Mean accuracy of the prediction of the covarying components of monkeys (Component 1 (C1) for Monkey H, Components 1 (C1) and 2 (C2) for Monkey S, and Components 1 (C1), 2 (C2) and 3 (C3) for Monkey J). The filled circles depict the correlation coefficient (B) and FVAF (C) between the actual and predicted profiles from the data. The open circles depict the correlation coefficient (B) and FVAF (C) between the actual profile and the profile predicted from random shuffling of ECoG signals. Error bars represent the S.E. $*p < 0.05$ (adjusted for multiple testing using the Holm method (n = 2)). (**D**) Reconstruction of the covarying component using ECoG signals during natural whole-body movement (Monkey H, free movement in the cage). The diagram uses a similar format for Fig. 6A. (**E**, **F**) Mean accuracy of the prediction of the covarying components of monkeys (Component 1 (C1) for Monkey H, Components 1 (C1) and 2 (C2) for Monkeys S and J). The diagram uses a similar format for Fig. 6B and C.

apparent for beta and gamma activity (Supplementary Figs. 5 and 6). These results suggest that high-gamma activity in the M1 was the most informative for decoding muscle activity during natural whole-body movement as well as forced forelimb movement.

3.6. A larger area of the sensorimotor cortex contributes to decoding during natural whole-body movement than forced forelimb movement

The color maps in Fig. 9A and C indicate that more electrodes

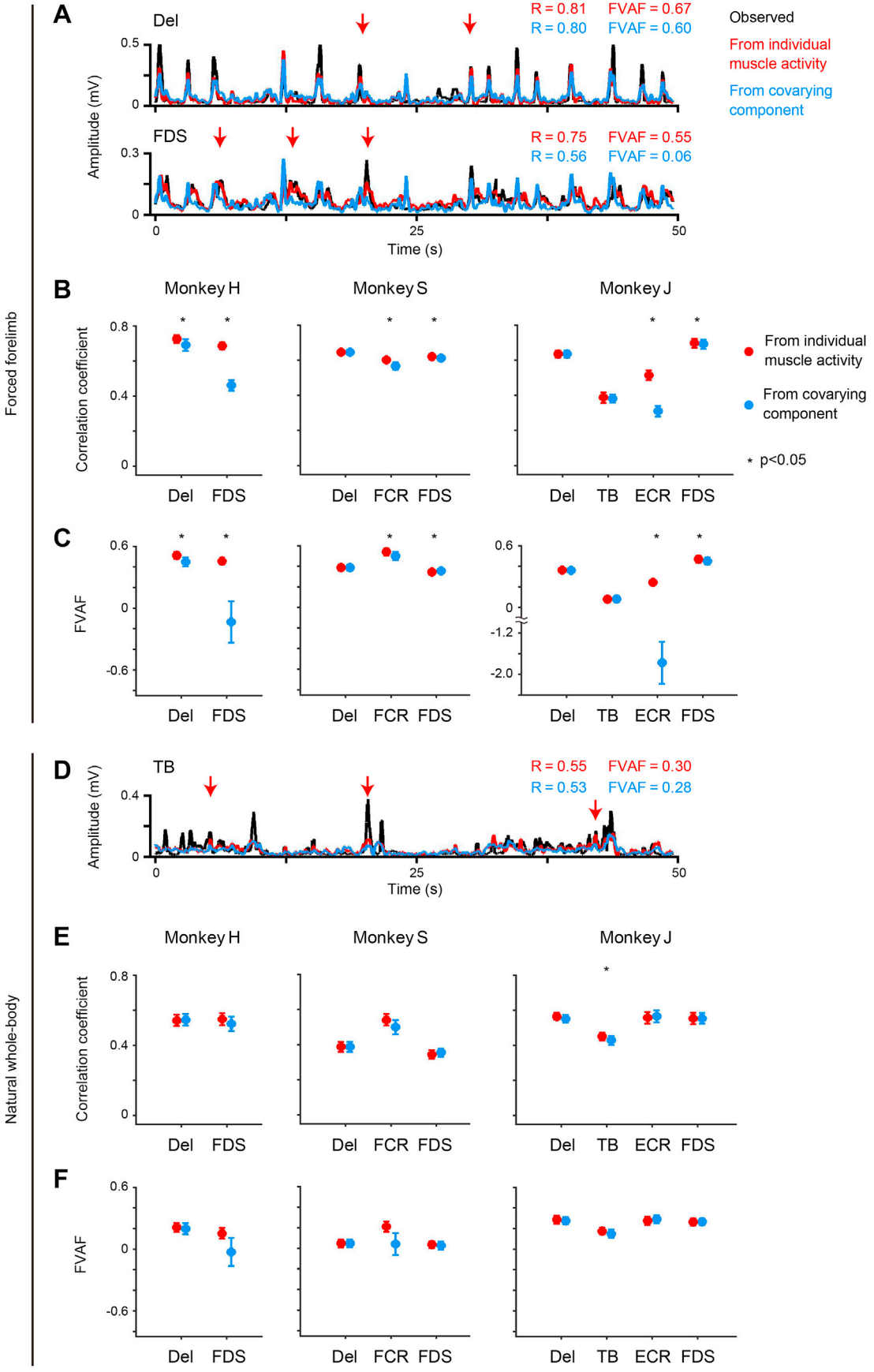

(caption on next page)

Fig. 7. Comparison of prediction performance of models derived from the individual muscle activity and that from the covarying component among multiple muscles. (**A**) Reconstruction of the shoulder (Del) and hand (FDS) muscle activities using ECoG signals during forced forelimb movement (Monkey H, the lever-pull task). The black trace shows the observed EMG profile. Red and cyan traces show EMG profiles predicted by models derived from individual muscle activity and the covarying component, respectively. The correlation coefficient (R) and FVAF between the observed and predicted EMG profiles are shown in the upper right corner of each graph. Arrows indicate typical points at which a model derived from individual muscle activity reconstructed the EMG profile better than those derived from the covarying component. (**B**, **C**) Mean accuracy of the prediction of each muscle activity. The filled circles depict the correlation coefficient (B) and FVAF (C) between the actual and predicted profiles from the data. Red and cyan circles show the performance of models derived from the individual muscle activity and the covarying component, respectively. Error bars represent the S.E. $*p < 0.05$ (adjusted for multiple testing using the Holm method (n = 2)). (**D**) Reconstruction of the elbow (TB) muscle activity using ECoG signals during natural whole-body movement (Monkey J). The diagrams use a similar format for Fig. 7A. (**E**, **F**). Mean accuracy of the prediction of each muscle activity. The diagrams use a similar format for Fig. 7B and C.

contributed to the decoding of muscle activity during natural whole-body movement than during forced forelimb movement. To verify this, we explored the proportion of electrodes that were selected by the SLiR for exhibiting high-gamma activity. First, we examined all electrodes positioned over the sensorimotor cortex. More electrodes showed a significant contribution to the decoding of EMG during natural whole-body movement than during forced forelimb movement (Supplementary Table 4). This was the case for only positive contribution (Fig. 10A), which suggests that a larger area of the sensorimotor cortex contributed to decoding during natural whole-body movement than during forced forelimb movement. However, neither beta nor gamma activity showed any difference in the number of selected electrodes between two types of behavior (Supplementary Fig. 7 and Supplementary Tables 5 and 6). Next, we compared the contribution of the electrodes located over three discrete regions to the decoding of muscle activity (the M1, premotor cortex, or S1). Over the M1, we found no difference in the number of electrodes that contributed to decoding for forced forelimb vs. natural whole-body movements (Fig. 10B). However, electrodes over both the premotor cortex and S1 showed a higher proportion of positive contributions to decoding during natural whole-body movement than during forced forelimb movement (Fig. 10C and D). These results indicate that the premotor cortex and S1 processed more information about muscle activity during natural whole-body movement than during forced forelimb movement. We confirmed this result by examining covariation between high-gamma activity and muscle activity using a correlational analysis on single channels; we found that high-gamma activity over the premotor cortex and S1 was more covariate with muscle activity during natural whole-body movement than during forced forelimb movement (Supplementary Fig. 8). Therefore, a larger cortical area, including the premotor cortex and S1, contributes to decoding during natural whole-body movement than during forced forelimb movement.

3.7. Generalization of models between forced forelimb movement and natural whole-body movement was not achieved

A number of previous studies have reported the successful decoding of muscle activity during repetitive movements (Flint et al., 2012a; Morrow and Miller, 2003; Pohlmeyer et al., 2007; Shin et al., 2012). It is not yet clear whether these results can be generalized to other behaviors, particularly natural behavior in daily life. To address this point, we compared the models in terms of generalization performance. We first assessed the generalization performance of models across different sessions for the same movement. Both indices of the prediction accuracy were better than those obtained from surrogate shuffled control data for a part of muscles (3 muscles in forced forelimb movement and 4 muscles in natural whole-body movement; Fig. 11; $p < 0.05$). We next assessed generalization performance of models across two types of movements. The correlation coefficient of the model's prediction was better than that obtained from surrogate shuffled control data for most of the muscles (Fig. 11A and C), but the FVAF of the model's prediction was not better than that obtained from surrogate shuffled control data for all the muscles (Fig. 11B and D). Furthermore, generalization performance between different sessions for the same movement was significantly better than that between two types of movements (8 muscles in forced forelimb movement and 7 muscles in natural whole-body movement, Fig. 11). These results suggested that the model obtained from data in forced forelimb movement could not be appropriately applied to natural whole-body movement, and vice versa.

4. Discussion

In the present study, we simultaneously recorded cortical and muscle activities in freely moving marmosets. We demonstrated that muscle activity during forced forelimb movement could be decoded from ECoG signals recorded over the sensorimotor cortex of marmosets, as is the case

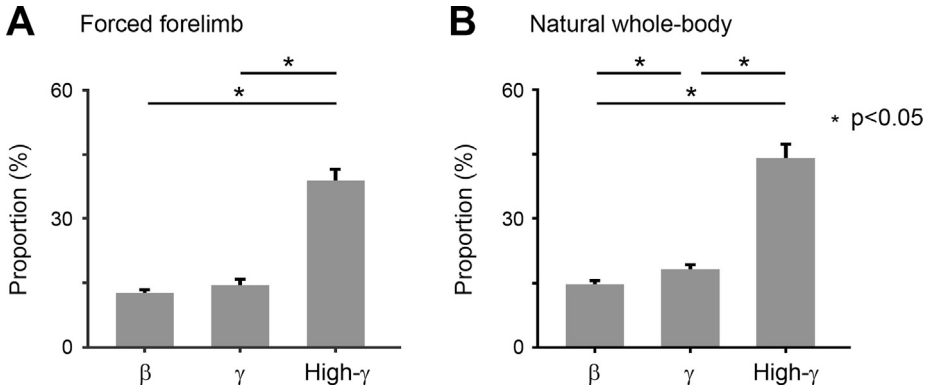

Fig. 8. The contribution of each frequency band in the prediction of muscle activity. (**A**, **B**) Each bar represents the proportion of electrodes selected by the SLiR in the prediction of muscle activity from respective frequency bands during forced forelimb (A) and natural whole-body movements (B). Error bars represent the S.E. (n = 9 muscles from three monkeys). $*p < 0.05$ (adjusted for multiple testing using the Holm method (n = 2)).

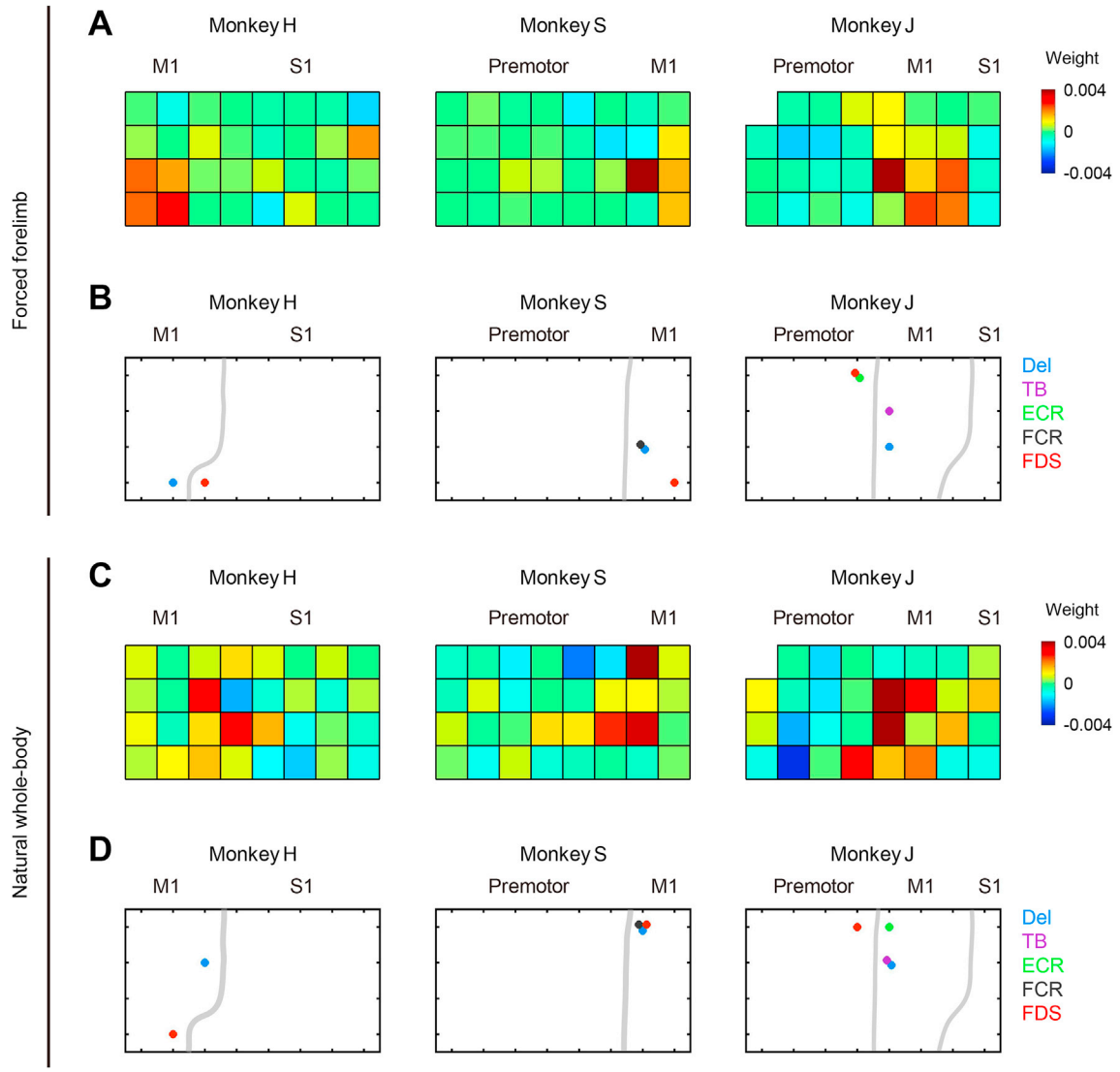

Fig. 9. The contribution of high-gamma activity recorded in each electrode to the prediction of muscle activity. (**A**, **C**) Color maps represent the weight values of high-gamma activity at each electrode on the grid in models that predict the activity of a shoulder muscle (Del) during forced forelimb (A) and natural whole-body movements (C). (**B**, **D**) The position of the electrode with the largest positive weight value in the model during forced forelimb (B) and natural whole-body movements (D). Colors represent muscles activity of which were predicted by the model (Del: blue; TB: purple; ECR: green; FCR: gray; FDS: red).

with other species (Nakanishi et al., 2017; Shin et al., 2012). We also found that the model could be used to successfully reconstruct muscle activity recorded during natural whole-body movement. For both forced and natural movements, high-gamma activity in the M1 was identified to be the most informative signal for decoding. A larger area of the sensorimotor cortex contributed significantly to the decoding of muscle activity during natural whole-body movement than during forced forelimb movement. Furthermore, generalization performance of the models across two types of movements was not achieved. These results indicate that while a linear combination of ECoG signals yields muscle activity during both forced forelimb and natural whole-body movements, cortical signals from a larger area are required for the decoding of muscle activity during natural whole-body movement. This suggests that decoding models obtained using the forced, repetitive behavior in many earlier reports may be specific to that type of movement, and cannot be generalized to other types of movement, such as free movement.

4.1. Models for forced forelimb and natural whole-body movements: common features

We detected a number of common features of models for forced forelimb and natural whole-body movements. First, high-gamma activity better predicted muscle activity than beta and gamma activities. High-gamma activity in local field potentials is considered to represent the summation of the synaptic transmission near the recording electrode (Buzsaki et al., 2012; Crone et al., 1998; Ray et al., 2008), and hence is indicative of neuronal activity near the electrode. Since an ensemble of neuronal activity in the sensorimotor cortex is known to encode muscle activity (Cherian et al., 2011; Fitzsimmons et al., 2009; Morrow and Miller, 2003; Pohlmeyer et al., 2007), it is possible that high-gamma activity represents information about muscle activity. High-gamma activity in local field potentials or ECoG signals is known to contribute to the decoding of muscle activity, kinematics, and forces during reaching movements in rhesus monkeys and humans (Chao et al., 2010; Flint et al., 2012b, 2014, 2017; Milekovic et al., 2015; Rickert et al., 2005; Shin

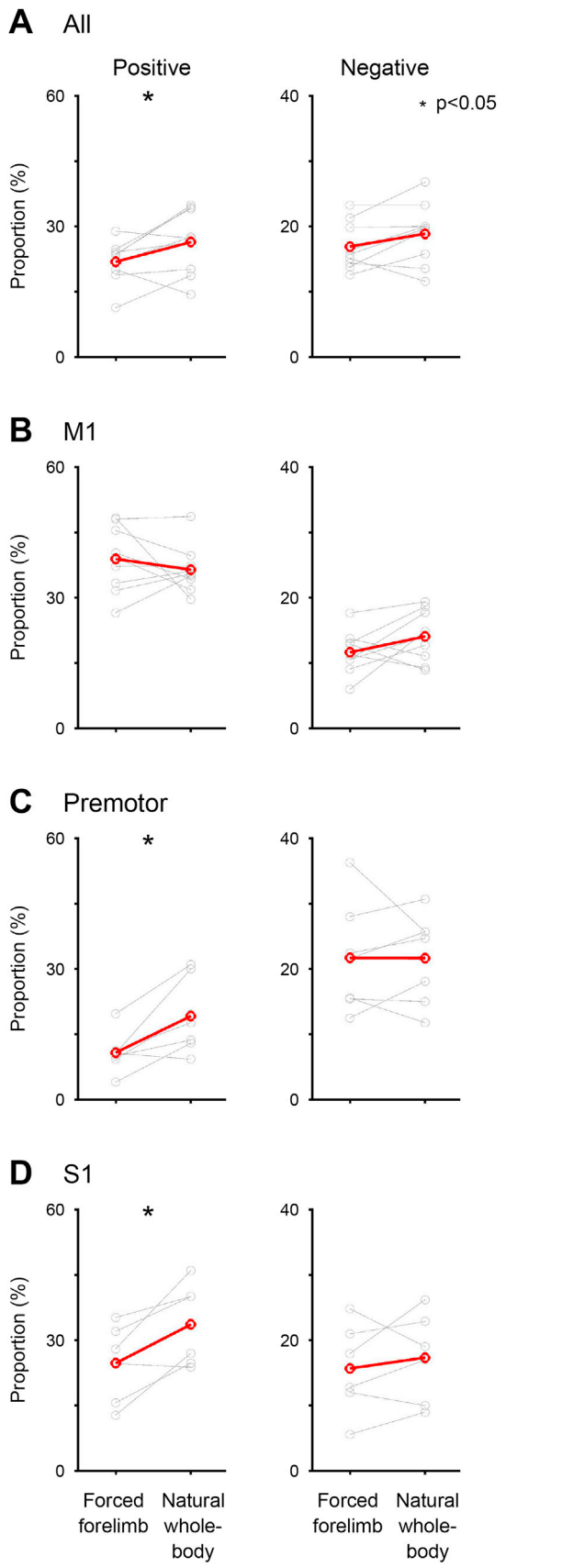

(caption on next column)

Fig. 10. Comparison of models for between forced forelimb movement and natural whole-body movement. (**A**) Comparison of the proportion of high-gamma activity selected by the SLiR in the prediction of muscle activity during forced forelimb and natural whole-body movements. The left graph represents results from electrodes for which the weight value was positive in the model, and the right graph represents results from electrodes for which the weight value was negative in the model. The gray circles indicate the proportion of models for each muscle (n = 9 muscles from the three monkeys), and the red circles show the average of all the models. *$p < 0.05$. (**B**–**D**) Comparison of the proportion of selected high-gamma activity recorded from electrodes at the M1 (B), premotor cortex (C), and S1 (D) (M1: n = 9 muscles from the three monkeys; premotor cortex: n = 7 muscles from two monkeys; S1: n = 6 muscles from two monkeys). The diagrams use a similar format for Fig. 10A.

et al., 2012; Zhuang et al., 2010). Our findings not only confirm these previous results (Fig. 4), but also extend these findings to natural whole-body movement (Fig. 5). A lower contribution of beta and gamma activity to decoding muscle activity was also a common feature between both forced and free movements, which also supports previous findings in monkeys (Flint et al., 2012a; Shin et al., 2012). By contrast, it is well known that cortical activity in the sensorimotor cortex is synchronized with muscle activity at a lower (beta) frequency range during isometric contraction (Baker et al., 1997; Conway et al., 1995; Mima and Hallett, 1999). A lower contribution of the beta range (Fig. 8 and Supplementary Fig. 4) than the high-gamma range may suggest that beta band cortico-muscular coherence might play roles other than generating a global pattern of muscle activity.

For both types of movements, the M1 region provided the most useful information for decoding muscle activity. This is in agreement with previous studies (Ball et al., 2009; Flint et al., 2014; Nakanishi et al., 2017; Schalk et al., 2007; Shin et al., 2012). Additionally, we propose that the contribution of the M1 was not restricted to forced movement, but was also applicable to natural movement.

4.2. Models for forced forelimb and natural whole-body movements: independent features

We found a difference between the models for forced forelimb vs. natural whole-body movements, and there was a poor generalization performance of the models between the two movements. Specifically, the size of the cortical area that contributed to the decoding of muscle activity was different between these two movements; a larger area of the sensorimotor cortex was involved in natural whole-body movement than forced forelimb movement. This finding is somewhat unexpected given the well-known contribution of spinal and subcortical systems in eliciting locomotion (Kiehn, 2006; Orlovsky et al., 1999), which was the type of behavior most frequently observed when monkeys were freely moving in their cage (Fig. 3A, Supplementary Tables 1 and 2). However, recent studies have shown that the motor cortex is involved in leg movement control, even during natural walking (Artoni et al., 2017; DiGiovanna et al., 2016).

The fact that a larger area of the sensorimotor cortex contributed to the decoding of muscle activity during natural movement may be due to greater variability in both motor and sensory information during natural movement compared with forced movement. For example, the shape of the EMG profile during natural whole-body movement was more varied than that during forced forelimb movement (Supplementary Fig. 3). A previous report has indicated that more complex limb kinematics are associated with a greater number of neuronal populations required to decode the hindlimb kinematics (Fitzsimmons et al., 2009). Since muscle activity represents the output from the "final common pathway", greater variation in EMG profiles might reflect variable motor commands from a larger area of the motor cortex. Variable sensory inputs to the cerebral cortex may also play a role in this phenomenon. Since the sensorimotor cortex receives multimodal sensory information during movement

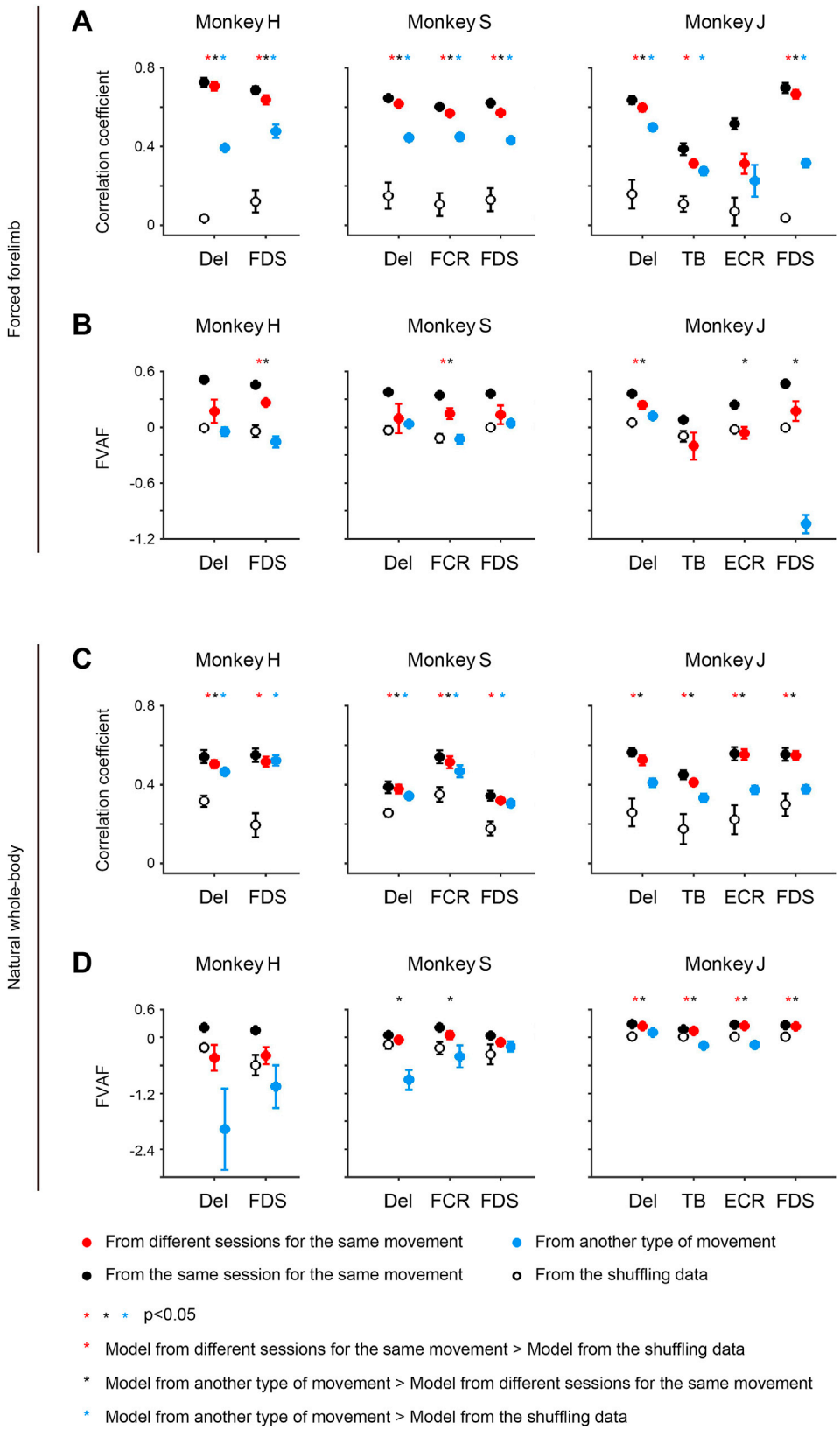

Fig. 11. Generalization performance of models between forced forelimb movement and natural whole-body movement. (**A**, **B**) Mean accuracy of the prediction of each muscle activity during forced forelimb movement. The filled black, red, cyan, and open circles depict prediction accuracy (A: the correlation coefficient; B: FVAF) of models obtained from data in the same session, data in different sessions for the same movement, data for another type of movement, and random shuffling data, respectively. Error bars represent the S.E. $*p < 0.05$ (adjustments for multiple testing using the Holm method ($n = 2$)). Some outliers in FVAF are not plotted in the graphs; TB of Monkey J: -6.0 ± 2.1 (mean ± S.E.); ECR of Monkey J: -9.5 ± 2.2. (**C**, **D**) Mean accuracy of the prediction of each muscle activity during natural whole-body movement. The diagrams use a similar format for Fig. 11A and B. An outlier in FVAF is not plotted in the graphs; FDS of Monkey J, -72.6 ± 6.3.

(Kuehn et al., 2018; Tkach et al., 2007; Waldert et al., 2015), the involvement of a larger area of the sensorimotor cortex might reflect richer sensory inputs provided by the external world to these cortical regions during the behavior in a naturalistic environment.

Generalization performance of the models between two types of movements was low (Fig. 11). This conclusion was based on the result of low FVAF values, which means that the models could not accurately predict the shape of the EMG profile. It is noteworthy, however, that the correlation coefficients derived from the model were better than those obtained from the surrogate shuffled control data. Since this correlation

coefficient was obtained from a whole 50-s epoch of data that contains a frequent alternation between active and non-active period, it may more preferentially represent the active period, rather than the EMG shape, of each behavior. In that case, it is possible that ECoG signals might preferentially encode the active period of ongoing behaviors, but not its quality, in a common way for both forced forelimb and natural whole-body movements. In any case, these results indicate that decoding performance is movement-specific.

4.3. Future applications

Various models of human diseases involving impaired movement have been developed with the common marmoset. These include models of artificial cerebral infarction (Bihel et al., 2010; Ikeda et al., 2013; Marshall and Ridley, 1996; Puentes et al., 2015; Virley et al., 2004), spinal cord injury (Bowes et al., 2013; Fouad et al., 2004; Iwanami et al., 2005; Kobayashi et al., 2012), and transgenic spinocerebellar ataxia (Tomioka et al., 2017). The applications of these models in preclinical research are limited, partly due to the challenges in evaluating their behavioral phenotypes using classical methods. Since these models inherently involve movement disorder/disability, monkeys may not be able to perform pre-trained movements. The ability to decode behaviors observed in freely moving animals will be useful for preclinical studies using these disease models because it does not require animals to perform any pre-trained movement.

The proposed decoding approach using a wireless recording system could potentially be applied to other species. Application in rodents would be especially advantageous because, unlike primates, an abundant number of human disease models have been established in rodents (Vandamme, 2015). Since individual techniques such as recording of muscle activity (Bercich et al., 2016) and cortical activity (Jia et al., 2018; Khorasani et al., 2016) using wireless recording from rodents have been independently reported, a combination of these technologies may enable analyses of cortical effects on movement in various disease models.

The proposed technique may also be applied to the field of BMI for human patients. One potential application is the functional electrical stimulation of muscles to move individual limbs. By generating electrical stimulus parameters based on predicted muscle activity, researchers have been able to use electrical stimulation to restore lost motor functions in tetraplegic patients and monkeys with a paralyzed hand (Ajiboye et al., 2017; Bouton et al., 2016; Ethier et al., 2012; Moritz et al., 2008). Another application could be the calculation of endpoint kinematics of prosthetic hands from muscle activity, using a similar algorithm to simulate limb kinematics from muscle activity (Crouch and He, 2015). According to the poor generalization performance between two types of movements found in the present study, decoders should ideally be built from data obtained under the same condition as the prosthetic hand is used. With the application of this technique to unrestrained, freely behaving patients, BMI techniques have an increased potential for improving the quality of life in patients with movement disorders.

Declarations of interest

None.

Acknowledgments

This work was supported by the program for Brain Mapping by Integrated Neurotechnologies for Disease Studies (Brain/MINDS) from the Japan Agency for Medical Research and Development, AMED, Japan.

Appendix A. Supplementary data

Supplementary data related to this article can be found at https://doi.org/10.1016/j.neuroimage.2019.04.045.

References

Aflalo, T.N., Graziano, M.S., 2006. Partial tuning of motor cortex neurons to final posture in a free-moving paradigm. Proc. Natl. Acad. Sci. U. S. A. 103, 2909–2914.
Ajiboye, A.B., Willett, F.R., Young, D.R., Memberg, W.D., Murphy, B.A., Miller, J.P., Walter, B.L., Sweet, J.A., Hoyen, H.A., Keith, M.W., Peckham, P.H., Simeral, J.D., Donoghue, J.P., Hochberg, L.R., Kirsch, R.F., 2017. Restoration of reaching and grasping movements through brain-controlled muscle stimulation in a person with tetraplegia: a proof-of-concept demonstration. Lancet 389, 1821–1830.
Artoni, F., Fanciullacci, C., Bertolucci, F., Panarese, A., Makeig, S., Micera, S., Chisari, C., 2017. Unidirectional brain to muscle connectivity reveals motor cortex control of leg muscles during stereotyped walking. Neuroimage 159, 403–416.
Baker, S.N., Olivier, E., Lemon, R.N., 1997. Coherent oscillations in monkey motor cortex and hand muscle EMG show task-dependent modulation. J. Physiol. 501 (Pt 1), 225–241.
Ball, T., Schulze-Bonhage, A., Aertsen, A., Mehring, C., 2009. Differential representation of arm movement direction in relation to cortical anatomy and function. J. Neural Eng. 6, 016006.
Bercich, R.A., Wang, Z., Mei, H., Hammer, L.H., Seburn, K.L., Hargrove, L.J., Irazoqui, P.P., 2016. Enhancing the versatility of wireless biopotential acquisition for myoelectric prosthetic control. J. Neural Eng. 13, 046012.
Bihel, E., Pro-Sistiaga, P., Letourneur, A., Toutain, J., Saulnier, R., Insausti, R., Bernaudin, M., Roussel, S., Touzani, O., 2010. Permanent or transient chronic ischemic stroke in the non-human primate: behavioral, neuroimaging, histological, and immunohistochemical investigations. J. Cereb. Blood Flow Metab. 30, 273–285.
Borton, D.A., Yin, M., Aceros, J., Nurmikko, A., 2013. An implantable wireless neural interface for recording cortical circuit dynamics in moving primates. J. Neural Eng. 10, 026010.
Bouton, C.E., Shaikhouni, A., Annetta, N.V., Bockbrader, M.A., Friedenberg, D.A., Nielson, D.M., Sharma, G., Sederberg, P.B., Glenn, B.C., Mysiw, W.J., Morgan, A.G., Deogaonkar, M., Rezai, A.R., 2016. Restoring cortical control of functional movement in a human with quadriplegia. Nature 533, 247–250.
Bowes, C., Burish, M., Cerkevich, C., Kaas, J., 2013. Patterns of cortical reorganization in the adult marmoset after a cervical spinal cord injury. J. Comp. Neurol. 521, 3451–3463.
Burish, M.J., Stepniewska, I., Kaas, J.H., 2008. Microstimulation and architectonics of frontoparietal cortex in common marmosets (Callithrix jacchus). J. Comp. Neurol. 507, 1151–1168.
Buzsaki, G., Anastassiou, C.A., Koch, C., 2012. The origin of extracellular fields and currents–EEG, ECoG, LFP and spikes. Nat. Rev. Neurosci. 13, 407–420.
Caminiti, R., Johnson, P.B., Urbano, A., 1990. Making arm movements within different parts of space: dynamic aspects in the primate motor cortex. J. Neurosci. 10, 2039–2058.
Capogrosso, M., Milekovic, T., Borton, D., Wagner, F., Moraud, E.M., Mignardot, J.B., Buse, N., Gandar, J., Barraud, Q., Xing, D., Rey, E., Duis, S., Jianzhong, Y., Ko, W.K., Li, Q., Detemple, P., Denison, T., Micera, S., Bezard, E., Bloch, J., Courtine, G., 2016. A brain-spine interface alleviating gait deficits after spinal cord injury in primates. Nature 539, 284–288.
Chao, Z.C., Nagasaka, Y., Fujii, N., 2010. Long-term asynchronous decoding of arm motion using electrocorticographic signals in monkeys. Front. Neuroeng. 3, 3.
Cherian, A., Krucoff, M.O., Miller, L.E., 2011. Motor cortical prediction of EMG: evidence that a kinetic brain-machine interface may be robust across altered movement dynamics. J. Neurophysiol. 106, 564–575.
Chestek, C.A., Gilja, V., Nuyujukian, P., Kier, R.J., Solzbacher, F., Ryu, S.I., Harrison, R.R., Shenoy, K.V., 2009. HermesC: low-power wireless neural recording system for freely moving primates. IEEE Trans. Neural Syst. Rehabil. Eng. 17, 330–338.
Cheung, V.C., Turolla, A., Agostini, M., Silvoni, S., Bennis, C., Kasi, P., Paganoni, S., Bonato, P., Bizzi, E., 2012. Muscle synergy patterns as physiological markers of motor cortical damage. Proc. Natl. Acad. Sci. U. S. A. 109, 14652–14656.
Conway, B.A., Halliday, D.M., Farmer, S.F., Shahani, U., Maas, P., Weir, A.I., Rosenberg, J.R., 1995. Synchronization between motor cortex and spinal motoneuronal pool during the performance of a maintained motor task in man. J. Physiol. 489 (Pt 3), 917–924.
Crone, N.E., Miglioretti, D.L., Gordon, B., Lesser, R.P., 1998. Functional mapping of human sensorimotor cortex with electrocorticographic spectral analysis. II. Event-related synchronization in the gamma band. Brain 121 (Pt 12), 2301–2315.
Crouch, D.L., He, H., 2015. Musculoskeletal model predicts multi-joint wrist and hand movement from limited EMG control signals. Conf Proc IEEE Eng Med Biol Soc 2015, 1132–1135.
DiGiovanna, J., Dominici, N., Friedli, L., Rigosa, J., Duis, S., Kreider, J., Beauparlant, J., van den Brand, R., Schieppati, M., Micera, S., Courtine, G., 2016. Engagement of the rat hindlimb motor cortex across natural locomotor behaviors. J. Neurosci. 36, 10440–10455.
Ethier, C., Oby, E.R., Bauman, M.J., Miller, L.E., 2012. Restoration of grasp following paralysis through brain-controlled stimulation of muscles. Nature 485, 368–371.
Fernandez-Leon, J.A., Parajuli, A., Franklin, R., Sorenson, M., Felleman, D.J., Hansen, B.J., Hu, M., Dragoi, V., 2015. A wireless transmission neural interface system for unconstrained non-human primates. J. Neural Eng. 12, 056005.
Fitzsimmons, N.A., Lebedev, M.A., Peikon, I.D., Nicolelis, M.A., 2009. Extracting kinematic parameters for monkey bipedal walking from cortical neuronal ensemble activity. Front. Integr. Neurosci. 3, 3.
Flint, R.D., Ethier, C., Oby, E.R., Miller, L.E., Slutzky, M.W., 2012a. Local field potentials allow accurate decoding of muscle activity. J. Neurophysiol. 108, 18–24.
Flint, R.D., Lindberg, E.W., Jordan, L.R., Miller, L.E., Slutzky, M.W., 2012b. Accurate decoding of reaching movements from field potentials in the absence of spikes. J. Neural Eng. 9, 046006.

Flint, R.D., Rosenow, J.M., Tate, M.C., Slutzky, M.W., 2017. Continuous decoding of human grasp kinematics using epidural and subdural signals. J. Neural Eng. 14, 016005.
Flint, R.D., Wang, P.T., Wright, Z.A., King, C.E., Krucoff, M.O., Schuele, S.U., Rosenow, J.M., Hsu, F.P., Liu, C.Y., Lin, J.J., Sazgar, M., Millett, D.E., Shaw, S.J., Nenadic, Z., Do, A.H., Slutzky, M.W., 2014. Extracting kinetic information from human motor cortical signals. Neuroimage 101, 695–703.
Foster, J.D., Nuyujukian, P., Freifeld, O., Gao, H., Walker, R., S, I.R., T, H.M., Murmann, B., J.B, M., Shenoy, K.V., 2014. A freely-moving monkey treadmill model. J. Neural Eng. 11, 046020.
Foster, J.D., Nuyujukian, P., Freifeld, O., Ryu, S.I., Black, M.J., Shenoy, K.V., 2012. A framework for relating neural activity to freely moving behavior. Conf Proc IEEE Eng Med Biol Soc 2012, 2736–2739.
Fouad, K., Klusman, I., Schwab, M.E., 2004. Regenerating corticospinal fibers in the Marmoset (Callitrix jacchus) after spinal cord lesion and treatment with the anti-Nogo-A antibody IN-1. Eur. J. Neurosci. 20, 2479–2482.
Ganesh, G., Burdet, E., Haruno, M., Kawato, M., 2008. Sparse linear regression for reconstructing muscle activity from human cortical fMRI. Neuroimage 42, 1463–1472.
Georgopoulos, A.P., Carpenter, A.F., 2015. Coding of movements in the motor cortex. Curr. Opin. Neurobiol. 33, 34–39.
Griffin, D.M., Hoffman, D.S., Strick, P.L., 2015. Corticomotoneuronal cells are "functionally tuned". Science 350, 667–670.
Ikeda, S., Harada, K., Ohwatashi, A., Kamikawa, Y., Yoshida, A., Kawahira, K., 2013. A new non-human primate model of photochemically induced cerebral infarction. PLoS One 8, e60037.
Iwanami, A., Yamane, J., Katoh, H., Nakamura, M., Momoshima, S., Ishii, H., Tanioka, Y., Tamaoki, N., Nomura, T., Toyama, Y., Okano, H., 2005. Establishment of graded spinal cord injury model in a nonhuman primate: the common marmoset. J. Neurosci. Res. 80, 172–181.
Jackson, A., Mavoori, J., Fetz, E.E., 2007. Correlations between the same motor cortex cells and arm muscles during a trained task, free behavior, and natural sleep in the macaque monkey. J. Neurophysiol. 97, 360–374.
Jaman, M.F., Huffman, M.A., 2008. Enclosure environment affects the activity budgets of captive Japanese macaques (Macaca fuscata). Am. J. Primatol. 70, 1133–1144.
Jia, Y., Khan, W., Lee, B., Fan, B., Madi, F., Weber, A., Li, W., Ghovanloo, M., 2018. Wireless opto-electro neural interface for experiments with small freely behaving animals. J. Neural Eng. 15, 046032.
Khorasani, A., Heydari Beni, N., Shalchyan, V., Daliri, M.R., 2016. Continuous force decoding from local field potentials of the primary motor cortex in freely moving rats. Sci. Rep. 6, 35238.
Kiehn, O., 2006. Locomotor circuits in the mammalian spinal cord. Annu. Rev. Neurosci. 29, 279–306.
Kilner, J.M., Baker, S.N., Lemon, R.N., 2002. A novel algorithm to remove electrical cross-talk between surface EMG recordings and its application to the measurement of short-term synchronisation in humans. J. Physiol. 538, 919–930.
Kobayashi, Y., Okada, Y., Itakura, G., Iwai, H., Nishimura, S., Yasuda, A., Nori, S., Hikishima, K., Konomi, T., Fujiyoshi, K., Tsuji, O., Toyama, Y., Yamanaka, S., Nakamura, M., Okano, H., 2012. Pre-evaluated safe human iPSC-derived neural stem cells promote functional recovery after spinal cord injury in common marmoset without tumorigenicity. PLoS One 7, e52787.
Komatsu, M., Sugano, E., Tomita, H., Fujii, N., 2017. A chronically implantable bidirectional neural interface for non-human primates. Front. Neurosci. 11, 514.
Kuehn, E., Haggard, P., Villringer, A., Pleger, B., Sereno, M.I., 2018. Visually-driven maps in area 3b. J. Neurosci. 38, 1295–1310.
Lebedev, M.A., Crist, R.E., Nicolelis, M.A.L., 2008. Frontiers in NeuroscienceBuilding brain-machine interfaces to restore neurological functions. In: Nicolelis, M.A.L. (Ed.), Methods for Neural Ensemble Recordings. CRC Press/Taylor & Francis Taylor & Francis Group, LLC., Boca Raton (FL).
Lebedev, M.A., Nicolelis, M.A., 2017. Brain-Machine interfaces: from basic science to neuroprostheses and neurorehabilitation. Physiol. Rev. 97, 767–837.
Loeb, G.E., Gans, C., 1986. Electromyography for Experimentalists. The University of Chicago Press.
Marshall, J.W., Ridley, R.M., 1996. Assessment of functional impairment following permanent middle cerebral artery occlusion in a non-human primate species. Neurodegeneration 5, 275–286.
Mavoori, J., Jackson, A., Diorio, C., Fetz, E., 2005. An autonomous implantable computer for neural recording and stimulation in unrestrained primates. J. Neurosci. Methods 148, 71–77.
Milekovic, T., Truccolo, W., Grun, S., Riehle, A., Brochier, T., 2015. Local field potentials in primate motor cortex encode grasp kinetic parameters. Neuroimage 114, 338–355.
Mima, T., Hallett, M., 1999. Corticomuscular coherence: a review. J. Clin. Neurophysiol. 16, 501–511.
Moritz, C.T., Perlmutter, S.I., Fetz, E.E., 2008. Direct control of paralysed muscles by cortical neurons. Nature 456, 639–642.
Morrow, M.M., Miller, L.E., 2003. Prediction of muscle activity by populations of sequentially recorded primary motor cortex neurons. J. Neurophysiol. 89, 2279–2288.
Moxon, K.A., Foffani, G., 2015. Brain-machine interfaces beyond neuroprosthetics. Neuron 86, 55–67.
Nakanishi, Y., Yanagisawa, T., Shin, D., Kambara, H., Yoshimura, N., Tanaka, M., Fukuma, R., Kishima, H., Hirata, M., Koike, Y., 2017. Mapping ECoG channel contributions to trajectory and muscle activity prediction in human sensorimotor cortex. Sci. Rep. 7, 45486.
Newman, J.D., Kenkel, W.M., Aronoff, E.C., Bock, N.A., Zametkin, M.R., Silva, A.C., 2009. A combined histological and MRI brain atlas of the common marmoset monkey, Callithrix jacchus. Brain Res. Rev. 62, 1–18.
Okano, H., Hikishima, K., Iriki, A., Sasaki, E., 2012. The common marmoset as a novel animal model system for biomedical and neuroscience research applications. Semin. Fetal Neonatal Med. 17, 336–340.
Orlovsky, G.D., Deliagina, T.G., Grillner, S., 1999. Neuronal Control of Locomotion. From Mollusc to Man. Oxford Univ. Press.
Pohlmeyer, E.A., Solla, S.A., Perreault, E.J., Miller, L.E., 2007. Prediction of upper limb muscle activity from motor cortical discharge during reaching. J. Neural Eng. 4, 369–379.
Prins, N.W., Pohlmeyer, E.A., Debnath, S., Mylavarapu, R., Geng, S., Sanchez, J.C., Rothen, D., Prasad, A., 2017. Common marmoset (Callithrix jacchus) as a primate model for behavioral neuroscience studies. J. Neurosci. Methods 284, 35–46.
Prins, N.W., Sanchez, J.C., Prasad, A., 2014. A confidence metric for using neurobiological feedback in actor-critic reinforcement learning based brain-machine interfaces. Front. Neurosci. 8, 111.
Puentes, S., Kaido, T., Hanakawa, T., Ichinohe, N., Otsuki, T., Seki, K., 2015. Internal capsule stroke in the common marmoset. Neuroscience 284, 400–411.
Rajangam, S., Tseng, P.H., Yin, A., Lehew, G., Schwarz, D., Lebedev, M.A., Nicolelis, M.A., 2016. Wireless cortical brain-machine interface for whole-body navigation in primates. Sci. Rep. 6, 22170.
Ray, S., Hsiao, S.S., Crone, N.E., Franaszczuk, P.J., Niebur, E., 2008. Effect of stimulus intensity on the spike-local field potential relationship in the secondary somatosensory cortex. J. Neurosci. 28, 7334–7343.
Rickert, J., Oliveira, S.C., Vaadia, E., Aertsen, A., Rotter, S., Mehring, C., 2005. Encoding of movement direction in different frequency ranges of motor cortical local field potentials. J. Neurosci. 25, 8815–8824.
Rosa, M.G., Tweedale, R., 2005. Brain maps, great and small: lessons from comparative studies of primate visual cortical organization. Philos. Trans. R. Soc. Lond. B Biol. Sci. 360, 665–691.
Schalk, G., Kubanek, J., Miller, K.J., Anderson, N.R., Leuthardt, E.C., Ojemann, J.G., Limbrick, D., Moran, D., Gerhardt, L.A., Wolpaw, J.R., 2007. Decoding two-dimensional movement trajectories using electrocorticographic signals in humans. J. Neural Eng. 4, 264–275.
Schwartz, A.B., 2016. Movement: how the brain communicates with the world. Cell 164, 1122–1135.
Schwarz, D.A., Lebedev, M.A., Hanson, T.L., Dimitrov, D.F., Lehew, G., Meloy, J., Rajangam, S., Subramanian, V., Ifft, P.J., Li, Z., Ramakrishnan, A., Tate, A., Zhuang, K.Z., Nicolelis, M.A., 2014. Chronic, wireless recordings of large-scale brain activity in freely moving rhesus monkeys. Nat. Methods 11, 670–676.
Shin, D., Watanabe, H., Kambara, H., Nambu, A., Isa, T., Nishimura, Y., Koike, Y., 2012. Prediction of muscle activities from electrocorticograms in primary motor cortex of primates. PLoS One 7, e47992.
Takei, T., Confais, J., Tomatsu, S., Oya, T., Seki, K., 2017. Neural basis for hand muscle synergies in the primate spinal cord. Proc. Natl. Acad. Sci. U. S. A. 114, 8643–8648.
Tia, B., Takemi, M., Kosugi, A., Castagnola, E., Ansaldo, A., Nakamura, T., Ricci, D., Ushiba, J., Fadiga, L., Iriki, A., 2017. Cortical control of object-specific grasp relies on adjustments of both activity and effective connectivity: a common marmoset study. J. Physiol. 595, 7203–7221.
Tkach, D., Reimer, J., Hatsopoulos, N.G., 2007. Congruent activity during action and action observation in motor cortex. J. Neurosci. 27, 13241–13250.
Tomioka, I., Ishibashi, H., Minakawa, E.N., Motohashi, H.H., Takayama, O., Saito, Y., Popiel, H.A., Puentes, S., Owari, K., Nakatani, T., Nogami, N., Yamamoto, K., Noguchi, S., Yonekawa, T., Tanaka, Y., Fujita, N., Suzuki, H., Kikuchi, H., Aizawa, S., Nagano, S., Yamada, D., Nishino, I., Ichinohe, N., Wada, K., Kohsaka, S., Nagai, Y., Seki, K., 2017. Transgenic monkey model of the polyglutamine diseases recapitulating progressive neurological symptoms. eNeuro 4.
Tresch, M.C., Cheung, V.C., d'Avella, A., 2006. Matrix factorization algorithms for the identification of muscle synergies: evaluation on simulated and experimental data sets. J. Neurophysiol. 95, 2199–2212.
Vandamme, T.F., 2015. Rodent models for human diseases. Eur. J. Pharmacol. 759, 84–89.
Virley, D., Hadingham, S.J., Roberts, J.C., Farnfield, B., Elliott, H., Whelan, G., Golder, J., David, C., Parsons, A.A., Hunter, A.J., 2004. A new primate model of focal stroke: endothelin-1-induced middle cerebral artery occlusion and reperfusion in the common marmoset. J. Cereb. Blood Flow Metab. 24, 24–41.
Waldert, S., Vigneswaran, G., Philipp, R., Lemon, R.N., Kraskov, A., 2015. Modulation of the intracortical LFP during action execution and observation. J. Neurosci. 35, 8451–8461.
Walker, J., MacLean, J., Hatsopoulos, N.G., 2017. The marmoset as a model system for studying voluntary motor control. Dev Neurobiol 77, 273–285.
Walker, J., Pirschel, F., Maclean, J.N., Hatsopoulos, N.G., 2018. Sensorimotor Cortical Population Responses across Natural Behaviors Annual Meeting of Society for Neuroscience.
Wang, Y., Fang, Q., Gong, N., 2014. Motor assessment of developing common marmosets. Neurosci Bull 30, 387–393.
Yin, M., Borton, D.A., Komar, J., Agha, N., Lu, Y., Li, H., Laurens, J., Lang, Y., Li, Q., Bull, C., Larson, L., Rosler, D., Bezard, E., Courtine, G., Nurmikko, A.V., 2014. Wireless neurosensor for full-spectrum electrophysiology recordings during free behavior. Neuron 84, 1170–1182.
Zhuang, J., Truccolo, W., Vargas-Irwin, C., Donoghue, J.P., 2010. Decoding 3-D reach and grasp kinematics from high-frequency local field potentials in primate primary motor cortex. IEEE Trans. Biomed. Eng. 57, 1774–1784.